 CMES, vol.8, no.1, pp.15-28, 2005

Reinforced 2d Domain Analysis Using BEM and Regularized BEM/FEM Combination

Alexandre S. Botta [1], **Wilson S. Venturini** [2]

Abstract: In this work a regularized boundary-finite element combination is proposed to analyse 2D elastostatic solids reinforced by fibres. The boundary element is adopted to model the matrix behaviour, while finite elements model the embedded fibres. The debonding effects caused by the adherence loss between the two materials are also considered. A three-degree polynomial is adopted to approach the displacement field along the fibre elements, while linear approximations are used to represent the bonding forces between fibres and the matrix. The non-linear debonding model is governed by a loading function written in terms of the contact forces and the relative displacements. The BEM algebraic equations are combined with the fibre finite element relations to eliminate the displacement unknowns along the interface. Then, the resulting redundant algebraic equations are eliminated by applying the least square procedure. An implicit non-linear scheme was proposed to model the debonding effects. Examples dealing with reinforced concrete elements are presented to illustrate the capability of the proposed model.

keyword: Boundary elements, reinforcements, BEM/FEM combination

1 Introduction

Since the direct boundary element approach has been formulated for elastostatics, Rizzo (1967) and Cruse (1969), this technique has experimented an enormous growth reaching nowadays almost all application fields in engineering. For the majority of the problems analysed with BEM the collocation scheme is the most employed one, which is justified by the simplicity to derive the integral representations.

In spite of using the standard collocation model to develop this work, it is important to mention other boundary integral methods that could also be adopted. The well-known Symmetric Galerkin Boundary Element Method (SGBEM) proposed in the eighties [Bonnet et al., 1998] has proved to be accurate and reliable to deal with many engineering problems. The drawback of this method is the evaluation of the hyper-singular elements always present in the formulation. Using the Meshless Local Petrov-Galerkin (MLPG) to solve non-hyper-singular displacement and traction integral equations is another elegant and reliable alternative that could be used to formulate the BEM/FEM coupling presented herein. This alternative avoids hyper-singular element integrals leading to simpler and more accurate procedure to compute the involved matrices. The weakly singular traction equation formulation was proposed by Okada, Rajiyah and Atluri (1989a,b). More recently, Han & Atluri (2003a,b) and Atluri et al. (2003) have proposed a more general formulation using the concepts of the Meshless Local Petrov-Galerkin – MLPG.

Although the BEM has demonstrated to be a very accurate and appropriate numerical tool for elastostatics, many times combining this technique with finite elements may be a more appropriate choice. The first works dealing with BEM-FEM combinations appeared in the end of seventies [Zienkiewicz, et al., 1977; Shaw & Falby, 1977 and Osias et al., 1977], where the technique has been adopted for simple cases characterized by the combination of sub-domains defined in the same space.

Two and three-dimensional solids reinforced by fibres, beams and even surface elements define a class of problems for which BEM/FEM combinations have been adopted in many situations [Vallabhan & Sivakumar, 1986, Coda & Venturini, 1995 and 1999, Coda et al., 1999 and Coda, 2001]. The BEM is often adopted to approximate the region described in the largest space, while

[1] São Carlos School of Engineering – University of São Paulo Av. Trabalhador São-Carlense, 400, 13566-970 – São Carlos, Brazil. alexbott@sc.usp.br

[2] São Carlos School of Engineering – University of São Paulo, Av. Trabalhador São-Carlense, 400, 13566-970 – São Carlos, Brazil. venturin@sc.usp.br

finite element equations are chosen to model structural elements defined in smaller spaces. Although recommended, this combination can exhibit unmatched coupling of some degrees of freedom what may bring numerical instabilities. This is always the case when an approximated boundary value of the finite element region is coupled with the corresponding value inside the BEM region.

Better results are always obtained using only BEM approach when the tractions along the interface are eliminated before the discretization, avoiding therefore any possible problem regarding the selected shape functions. This formulation has been first introduced by Venturini (1992) and recently extended to analyse thin inclusions, including fibres [Leite, et al., 2003]. Particularly for the case of fibre immersed into 2D solids, closed analytical forms to carry out all boundary and interface element integrals have been used, eliminating therefore any possible numerical integration error.

Herein, the standard BEM/FEM combination is again considered to analyse the simple case of fibres immersed in a two-dimensional domain. Boundary elements are adopted to describe the equilibrium of the two-dimensional domain. The algebraic equations of the fibres, assumed without any bending stiffness, are written using the finite element approach. The interface forces are considered as load lines to derive the 2D solid integral representations and as body forces for the fibre differential equation. A third degree polynomial is adopted to approach the displacement field along the fibre, leading to linear approximation for the interactive bonding forces. Algebraic equations are written for all nodes defined along the interface and required to approach the displacement field. The BEM algebraic block equation is combined with the finite element relations written for the fibre structure to eliminate the displacement unknowns along the interface. A debonding criteria is also assumed to governs the shear stresses along the fibre-matrix interface. An implicit scheme employing consistent tangent matrix was also developed to deal the non-linear case. In order to assure stability of the combined system of equations, a certain number of redundant relations for nodes taken along the interface is written. Then, the number of relations is properly reduced by using the least square concept.

Numerical examples are shown to illustrate the capability of both, the proposed enriched BEM-FEM combination and the degenerated sub-region technique, to deal with fibres immersed into two dimensional elastic solids, leading to very accurate results, without exhibiting spurious oscillations as often observed for this kind of problems.

2 Basic equations

Let us consider the domain Ω depicted in Figure 1 that, for simplicity but without loss of generality, is reinforced by a single fibre Ω_f.

For the elastic body Ω, the equilibrium equation written in terms of displacements is given by:

$$u_{i,jj}+\frac{1}{1-2\nu}u_{j,ji}+b_i/G=0 \tag{1}$$

where u_i represents displacement components, G is the shear modulus and ν is Poisson's ratio.

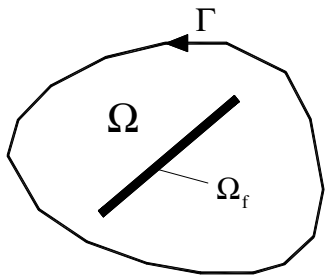

Figure 1 : Domain reinforced by single fibre.

As usual, for a domain Ω with boundary Γ, the integral representation of displacements is derived by applying Betti's principle (or Green's second identity).

$$c_{ij}u_j=-\int_\Gamma p^*_{ij}u_j d\Gamma+\int_\Gamma u^*_{ij}p_j d\Gamma+\int_{\Gamma_f} u^*_{is}f_s d\Gamma \tag{2}$$

where the symbols "$*$" is used to indicate fundamental solutions and p_j represent boundary traction values.

In equation (2) f_s is the internal force acting along the interface Γ_f and represents the fibre effects. They may be assumed as body forces multiplied by the fibre thickness. Thus, the fibre domain Ω_f depicted in Figure 1 is replaced by the interface Γ_f where f_s acts, as shown in Figure 2.

One can differentiate equation (2) to derive the integral representation of strains and then apply the Hooke's law

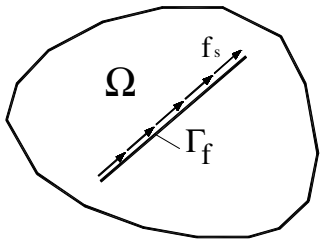

Figure 2 : Line load f_s acting along the interface Γ_f.

to obtain the stress integral equation, as follows,

$$\sigma_{ij}^k = -\int_\Gamma S_{ijk}^* u_k d\Gamma + \int_\Gamma D_{ijk}^* p_k d\Gamma + \int_{\Gamma_f} D_{ijs}^* f_s \tag{3}$$

where S_{ijk}^*, and D_{ijk}^* are well known tensors for the stress equation obtained by applying the Hooke's law on the fundamental solution at the source point, $D_{ijs}^* = D_{ijk}^* s_k$ being s_k the fibre cosine director (Brebbia & Dominguez, 1992).

For the fibre domain, Ω_f, the differential equation is very simple and given by:

$$\frac{d^2 u^f}{ds^2} + \frac{f^f}{E^f S} = 0 \tag{4}$$

where u^f is the displacement in the fibre direction, f^f is the distributed force applied along the fibre, representing the interface forces (bonding forces) when the element is immersed into a 2D or 3D body, and $E^f S$ gives the element rigidity (E^f and S are the elastic modulus and the cross section area of the fibre).

From the Virtual Work Principle one can find:

$$\int_{\Gamma_f} \overline{\varepsilon}\sigma d\Gamma = \int_{\Gamma_f} \overline{u} f^f d\Omega + \sum_{i=1}^{N_p} \overline{u}^i F^i \tag{5}$$

where σ is the fibre normal stress component, F^i gives the concentrated forces at N_p fibre end nodes i, while the upper bars indicate virtual strains and displacements in the fibre direction.

3 Debonding model

Fibres embedded in the domain (matrix material) can only pay important roles to modify the solid stiffness and loading capacity if enough internal forces along the interface can be sustained. Sliding along the interface may be allowed when a certain amount of strength is preserved. The ideal situation where perfect bonding is assumed is impossible in practice; at least in the vicinity of fibre ends, the interface forces tend to rise to infinity and therefore sliding occurs according to the bonding carrying capacity.

To model the slip that may occur in the matrix-fibre interface, a debonding criterion should be considered. In this work, the model proposed in the CEB-FIP (1990) was implemented together with the proposed BEM-FEM coupling. This model is particularly appropriate to simulate the concrete-steel debonding process in reinforced concrete members.

The curve shown in Figure 3 represents the debonding criterion obtained from the CEB-FIP (1990) to relate the bonding forces f with the slip s, which represents the relative displacement due to the sliding effects. The following parameters define this model: maximum bonding force $f_{\max}$, residual bonding force f_f, slip characteristic values s_1, s_2 and s_3, constant α and the unloading modulus S_d. These parameters, found in the CEB-FIP recommendations, are given in terms of the steel arrangements, bonding conditions and characteristic concrete strength in compression.

From the Figure 3, the following relationships can be written for the adopted model:

$$f = f_{\max}(s/s_1)^\alpha \qquad \text{for} \quad [0, s_1] \tag{6}$$

$$f = f_{\max} \qquad \text{for} \quad [s_1, s_2] \tag{7}$$

$$f = [f_{\max} \cdot s_3 - f_f \cdot s_2 + (f_f - f_{\max}) \cdot s]/(s_3 - s_2) \qquad \text{for} \quad [s_2, s_3] \tag{8}$$

$$f = f_f \qquad \text{for} \quad s > s_3 \tag{9}$$

4 Algebraic equations

4.1 Displacement compatibility and equilibrium equation

In order to analyse reinforced solids governed by the debonding model given in item 3, the relative displacements between fibres (steel bars for the reinforced concrete case) and the matrix (concrete material assumed homogeneous and isotropic) are taken into account to define the kinematic relationships. The displacements at matrix points along the interface are denoted by the vector u^i and

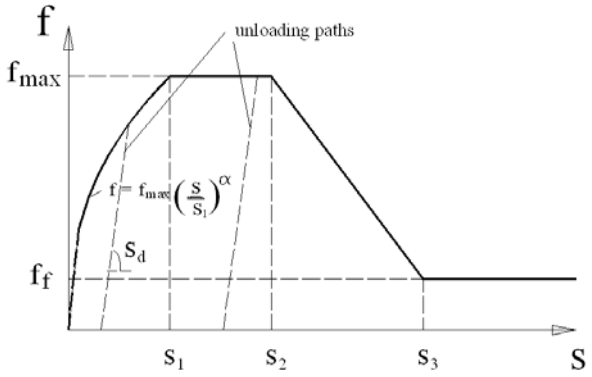

Figure 3 : CEB-FIP (1990) debonding model.

are represented algebraically by the BEM equations. On the other hand, the nodal displacements of the embedded fibres are denoted by the vector u^f. Then, assuming that a relative displacement along the interface may occur, the displacement compatibility reads:

$$u^f = u^i + s \tag{10}$$

being s the nodal slip values.

The equilibrium equation is represented by $f^f + f^i = 0$, where f^f and f^i are nodal value vectors of distributed forces applied to the fibre finite elements and acting along the interface line (bonding forces) in the 2D domain, respectively.

4.2 BEM equations

As usual for BEM formulations, algebraic equations are obtained from equations (2) and (3). One has to discretize both the boundary Γ of the 2D domain and the interface Γ_f into elements and approximate the associated variables, displacements and tractions along the boundary elements and interaction forces along the fibre interface elements. In the present case, continuous and discontinuous linear elements have been conveniently adopted.

From equation (2), one can write the algebraic representation for the displacements at any collocation point x defined inside the domain, along the fibre load line, along the boundary or outside, as follows:

$$c(x)u(x) = -H(x)U + G(x)P + S(x)f^i \tag{11}$$

where $H(x)$, $G(x)$ and $S(x)$ are influence matrices obtained by carrying out the integrals over boundary and interface elements in equation (2), $u(x)$ gives the displacement components at the collocation x and U and P are vectors containing boundary nodal displacements and tractions, respectively.

Selecting a proper number of collocation points along the boundary and along the interface, two sets of algebraic equations can be derived for boundary nodes and internal points, respectively, as follows:

$$H_b U = G_b P + S_b f^i \tag{12}$$

$$u^i = -H_i U + G_i P + S_i f^i \tag{13}$$

where the subscripts b and i indicate the block matrix for boundary and interface nodes, respectively.

Remark: very short elements to represent the fibre ends may be defined together with the corresponding interface forces. If considered, an extra degree of freedom must be defined at the middle point of those elements.

For the stresses, the algebraic equations are directly derived from the stress integral representation given by equation (3), as follows:

$$\sigma = -H' U + G' P + S' f^i \tag{14}$$

where H', G' and S' are obtained by carrying out the integrals over boundary and interface elements in equation (3).

It should be noted that special care is required when writing values that involve displacement derivatives, which is the case of stresses in equation (14). The collocations at the interface must be properly chosen and one has to compute correctly the Hadamard's finite parts when performing the integrals over adjacent elements.

4.3 FEM equations

From equation (5), one can write the algebraic equations using finite elements choosing properly the approximations of displacements and body forces (bonding forces) over each element. In this work, third degree polynomials are adopted to approximate the displacements along fibre elements; as a consequence of equation (4) the bonding forces are linearly approximated. Thus, for each fibre finite element, four nodes equally spaced along the fibre element length L are required for displacement approximation, while the bonding force approximation requires only two nodes. As the relationship between

slip and bonding force taken directly from the debonding model is locally defined, it is convenient to adopt the same linear approximation for the slip variable s, using also the same end nodes.

As usual adopted for BEM/FEM combination, the integral of the right hand side of equation (5) are performed keeping as nodal values the bonding force values. Thus, the obtained FEM matrix equation for a single fibre element is given by:

$$H^f u^f = G^f f^f + P^f \tag{15}$$

Substituting u^f according to equation (10) gives:

$$H^f u + H^s s = G^f f^f + P^f \tag{16}$$

where u^i was replaced by u, H^f and H^s are the fibre stiffness matrices, separately represented to take into account different approximations of u and s, G^f is the well-known lumping matrix, while P^f stands for applied nodal concentrated forces.

For the fibre element defined in Figure 4, the matrices H^f can be easily derived, as follows:

$$H^f = \frac{E^f S}{40L}\begin{bmatrix} 148 & -189 & 54 & -13 \\ -189 & 432 & -297 & 54 \\ 54 & -297 & 432 & -189 \\ -13 & 54 & -189 & 148 \end{bmatrix} \tag{17}$$

where $E^f S$ is the bar section rigidity.

The lumping matrix G_f appears when transforming the nodal forces (standard FEM formulations) into interface traction nodal values. It is obtained by performing the integral of the product of the third degree displacement approximating function ϕ and the linear approximation function ψ adopted for interface tractions, i.e., $G_f = \int_{\Gamma^f} \phi\psi dA$. For the fibre element defined in Figure 4, with linear function ψ for bonding forces and the third degree polynomial function ϕ for displacements, the lumping matrix G_f, given in terms of its geometrical characteristics, reads:

$$\left[G^f\right]^T = \begin{bmatrix} \frac{13L}{120} & \frac{3L}{10} & \frac{3L}{40} & \frac{L}{60} \\ \\ \frac{L}{60} & \frac{3L}{400} & \frac{3L}{10} & \frac{13L}{120} \end{bmatrix} \tag{18}$$

The matrix H^s is directly obtained from equation (17) by approximating linearly the displacement s to give:

$$\mathrm{H}^s = \frac{E^f S}{40L}\begin{bmatrix} 148 & -189 & 54 & -13 \\ -189 & 432 & -297 & 54 \\ 54 & -297 & 432 & -189 \\ -13 & 54 & -189 & 148 \end{bmatrix}$$

$$\begin{Bmatrix} s_1 \\ \frac{2}{3}s_1 + \frac{1}{3}s_2 \\ \frac{1}{3}s_1 + \frac{2}{3}s_2 \\ s_2 \end{Bmatrix} = \frac{E^f S}{L}\begin{bmatrix} 1 & -1 \\ 0 & 0 \\ 0 & 0 \\ -1 & 1 \end{bmatrix}\begin{Bmatrix} s_1 \\ s_2 \end{Bmatrix} \tag{19}$$

where s_1 and s_2 are nodal slip variables shown in Figure 4.

It is to be noted that the values $(2s_1/3 + s_2/3)$ and $(s_1/3 + 2s_2/3)$ that appear in equation (19) are the s values computed at the element thirds.

4.4 BEM/FEM combination

In order to combine the algebraic equations obtained from both BEM and FEM schemes applied to the matrix body and to bars or fibres, respectively, one has to enforce traction equilibrium and displacement compatibility at the interface nodes, i.e., $u^f = u^i + s$ and $f^i + f^f = 0$, bearing in mind that, along the interface, the displacements and interface shear tractions are the unknown values.

For N selected collocation points related with the N boundary nodes, equation (12) contains $2N$ boundary algebraic relationships, relating $2N$ displacements U and $2N$ tractions P, and a certain number of internal matrix-fibre interface unknowns, contained in f^i, necessarily smaller than $2M$ the corresponding dimension of matrix-fibre interface displacement vector u^i. To couple BEM domains with fibre reinforcement, equation (13) has to be written for the M collocation points defined along the fibre where displacement compatibility is enforced, giving $2M$ algebraic relations. Moreover, if convenient to improve numerical solutions, other redundant displacement equations can be written for complementary collocations defined along the fibre elements, but without introducing new unknowns. The dimension $2M$ of H_i can be therefore conveniently increased. The displacement values at the new collocations are properly replaced by considering the approximation function along the fibre element. The number of redundant equations will be larger than $2M$, but the number of displacement values remains $2M$,

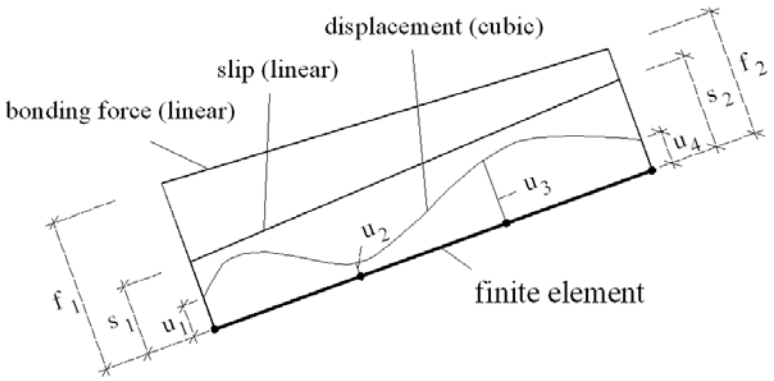

Figure 4 : Variable approximations for fibre element.

while the number of nodal bonding forces is smaller that $2M$.

As described above and also illustrated in Figure 4, at the fibre element level, the number of displacement values is much larger than that of bonding force values. Thus, in equation (13) the number of algebraic relations is much larger than the number of force values in f^i. To reduce the number of equations to be equal to the number of unknowns one can apply the least square method. In this work, we have simplified this scheme reducing the number of equations at element level. Equation (13) was rewritten to express the displacement values at nodes defined over a single fibre, as follows:

$$u_k = -H_k U + G_k P + S_k f^i \tag{20}$$

where $k = 1, \cdots, n$ is the fibre number and the matrices H_k, G_k and $S_k$are now referred to the fibre k.

To reduce the redundant algebraic relations, in equation (20) one has to use the least square method leading to the following reduced system of equations:

$$S_k^T u_k = -S_k^T H_k U + S_k^T G_k P + S_k^T S_k f^i \tag{21}$$

where the matrix S_k is defined for each fibre and S_k^T is its transpose matrix.

Equations (21) written for all fibres are joined together to define the system of algebraic relations for the interface points. The final number of algebraic relations written for interface nodes is exactly the dimension of vector f^i. After applying the boundary conditions, all relations for the interface points are expressed by,

$$Su^i = -HU + GP + Rf^i \tag{22}$$

where the matrices S, H, G and R are properly obtained from equation (21).

It is important to point out that, in equation (22), the boundary conditions have already been introduced therefore the matrices H and G contains displacement and tractions coefficients. For simplicity, the notation U is referred to the boundary unknowns and P refers to the prescribed boundary values.

Equation (22) is a regularized algebraic representation relating boundary and bonding force unknowns.

Similarly, applying the boundary conditions to the boundary algebraic system of equations (12) gives:

$$U = H_b^{-1} G_b P + R_b f^i \tag{23}$$

where $R_b = H_b^{-1} S_b$ stands for the bonding forces influences.

Replacing the unknown vector U in equation (22) leads to:

$$Su^i = (G - HH_b^{-1} G_b) P + (R - HR_b) f^i \tag{24}$$

or simply

$$Su^i = \overline{G} P + \overline{S} f^i \tag{25}$$

where

$$\overline{G} = G - HH_b^{-1} G_b \tag{26}$$

$$\overline{S} = R - HR_b \tag{27}$$

The regularized BEM equation (25), containing only internal unknowns, can be combined with the FEM algebraic equation (16), by enforcing displacement compatibility ($u^f = u^i + s$) and equilibrium ($f^i = -f^f$) conditions

to give the final algebraic representation of the reinforced solid as follows:

$$\begin{bmatrix} S & 0 \\ H^f & H^s \end{bmatrix} \begin{Bmatrix} u \\ s \end{Bmatrix} = \begin{bmatrix} \overline{G} \\ 0 \end{bmatrix} \{P\} + \begin{bmatrix} \overline{S} \\ -G^f \end{bmatrix} f + \begin{Bmatrix} 0 \\ P^f \end{Bmatrix} \tag{28}$$

where, for convenience, the index i has been suppressed.

5 Non-linear formulation

To solve equation (28), one has to take into account the non-linear relationship described by the debonding model presented in item 3, in which the relation between the debonding force f and the slip s, $f = f(s)$ is established. The equilibrium equation (28) is then rewritten in terms of the variable increments, as follows:

$$\begin{bmatrix} S & 0 \\ H^f & H^s \end{bmatrix} \begin{Bmatrix} \Delta u_n \\ \Delta s_n \end{Bmatrix} = \begin{bmatrix} \overline{G} \\ 0 \end{bmatrix} \{\Delta P_n\} + \begin{bmatrix} \overline{S} \\ -G^f \end{bmatrix} \{\Delta f_n(\Delta s_n)\} + \begin{Bmatrix} 0 \\ \Delta P_n^f \end{Bmatrix} \tag{29}$$

where for any value a, $\Delta a_n = a_{n+1} - a_n$ is its increment in the time increment Δt_n.

From equation (29) one can find the unknown vector $\begin{Bmatrix} \Delta u_n & \Delta s_n \end{Bmatrix}^T$, as follows:

$$\begin{Bmatrix} \Delta u_n \\ \Delta s_n \end{Bmatrix} = [K] \begin{bmatrix} \overline{G} \\ 0 \end{bmatrix} \{\Delta P_n\} + [K] \begin{bmatrix} \overline{S} \\ -G^f \end{bmatrix} \{\Delta f_n(\Delta s_n)\} + [K] \begin{Bmatrix} 0 \\ \Delta P_n^f \end{Bmatrix} \tag{30}$$

where

$$[K] = \begin{bmatrix} S & 0 \\ H^f & H^s \end{bmatrix}^{-1} \tag{31}$$

Equation (30) can be conveniently rewritten in the following form:

$$\begin{Bmatrix} \Delta u_n \\ \Delta s_n \end{Bmatrix} = \begin{bmatrix} K_{uu} \\ K_{su} \end{bmatrix} \overline{G} \Delta P_n + \begin{bmatrix} K_{uu} & K_{us} \\ K_{su} & K_{ss} \end{bmatrix} \begin{bmatrix} \overline{S} \\ -G^f \end{bmatrix} \Delta f_n(\Delta s_n) + \begin{bmatrix} K_{us} \\ K_{ss} \end{bmatrix} \Delta P_n^f \tag{32}$$

where K_{ik} are sub-matrices of K, conveniently rearranged to compute Δu_n and Δs_n, respectively.

From equation (32), one can write separately the slip increment Δs_n as follows:

$$\Delta s_n = K_{su} \overline{G} \Delta P_n + [K_{su} \; K_{ss}] \begin{bmatrix} \overline{S} \\ -G^f \end{bmatrix} \Delta f_n(\Delta s_n) + K_{ss} \Delta P_n^f \tag{33}$$

Rearranging equation (33) one obtains:

$$Y(\Delta s_n) = \Delta s_n - \left[\overline{K}_{su} \; K_{ss}\right] \begin{Bmatrix} \Delta P_n \\ \Delta P_n^f \end{Bmatrix} - S_s \Delta f_n(\Delta s_n) = 0 \tag{34}$$

where

$$S_s = [K_{su} \; K_{ss}] \begin{bmatrix} \overline{S} \\ -G^f \end{bmatrix} \tag{35}$$

$$\overline{K}_{su} = K_{su} \overline{G} \tag{36}$$

Equation (34) represents a non-linear system of equations given in terms of the slip increment $\{\Delta s_n\}$. It can be solved by applying the Newton-Raphson scheme. An iterative process may be required to achieve the equilibrium. Then, from the iteration i the next try, $i+1$, for the time increment Δt_n is given by:

$$\Delta s_n^{i+1} = \Delta s_n^i + \delta \Delta s_n^i \tag{37}$$

Linearizing equation (34) and using the first term of the Taylor's expansion, give:

$$Y\left(\Delta s_n^i\right) + \frac{\partial Y\left(\Delta s_n^i\right)}{\partial \Delta s_n^i} \delta \Delta s_n^i + \cdots = 0 \tag{38}$$

The derivative that appears in equation (38) is directly obtained from equation (34) using the debonding model relationships given by equations (6)-(9). Then, one has:

$$\frac{\partial Y\left(\Delta s_n^i\right)}{\partial \Delta s_n^i} = I - S_s \left[\frac{\partial \Delta f_n\left(\Delta s_n^i\right)}{\partial \Delta s_n^i}\right] = S^{CTO} \tag{39}$$

where I is the identity matrix.

The matrix S^{CTO}, in equation (39), is the algorithmic consistent tangent operator for the present formulation. The derivatives on the right hand side of equation (39) depend on the actualized slip values, $s_{n+1}^i = s_n + \Delta s_n^i$, computed

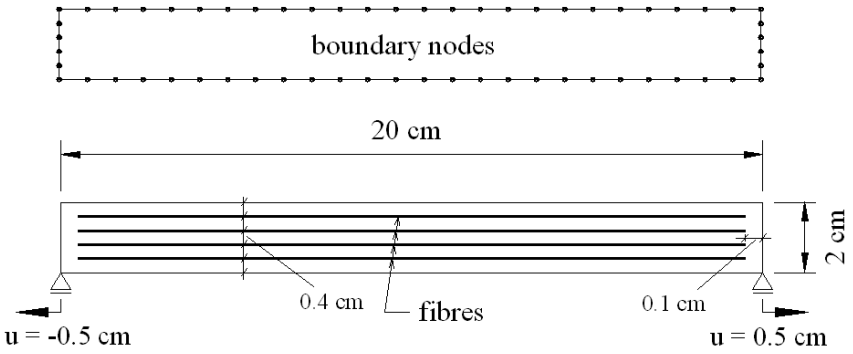

Figure 5 : Stretched reinforced domain. Geometry and discretization.

appropriately according to the intervals of s defined in equations (6)-(9). These derivatives are locally defined by:

$$\frac{d\left(\Delta f_n\left(\Delta s_n^i\right)\right)}{d\Delta s_n^i} = \frac{\alpha f_{\max}}{s_1}\left(\frac{\left(s_n+\Delta s_n^i\right)}{s_1}\right)^{\alpha-1} \quad \text{for} \quad [0,s_1] \tag{40}$$

$$\frac{d\left(\Delta f_n\left(\Delta s_n^i\right)\right)}{d\Delta s_n^i} = 0 \qquad \text{for} \quad [s_1,s_2] \tag{41}$$

$$\frac{d\left(\Delta f_n\left(\Delta s_n^i\right)\right)}{d\Delta s_n^i} = \frac{(f_f - f_{\max})}{(s_3-s_2)} \qquad \text{for} \quad [s_2,s_3] \tag{42}$$

$$\frac{d\left(\Delta f_n\left(\Delta s_n^i\right)\right)}{d\Delta s_n^i} = 0 \qquad \text{for} \quad s > s_3 \tag{43}$$

Reaching the convergence in equation (34) for the time increment Δt_n after i iterations, one has to compute the slip variable s to start the next increment, as follows:

$$s_{n+1} = s_n + \Delta s_n^i \tag{44}$$

After finding $\Delta s_n = s_{n+1} - s_n$, other variables are directly obtained. The internal displacements in Δu_n are computed from the first block in equation (32). The debonding forces are computed from the constitutive relation $\Delta f_n(\Delta s_n)$. The boundary displacements and tractions, stresses and strains in the 2D domain are computed by the appropriate integral equations.

6 Numerical examples

In this section, two numerical examples are analysed to check the performance and accuracy of the proposed BEM/FEM combination for two-dimensional reinforced solids.

The rectangular domain reinforced by four internal fibres, as shown in Figure 5, defines the first example. Plane stress conditions were assumed for the two-dimensional matrix domain, although according to its length/height ratio beam behaviour is expected. The matrix material is assumed linear elastic with Young's modulus $E_m = 2{,}000.0$ kN/cm^2 and Poisson's ratio $\nu = 0.0$. The rigidity associated with the matrix domain is given by $A_m E_m = 4{,}000.0$ kN, in which A_m is the corresponding matrix cross-section area, while the rigidity of each bar is $A_f E_f$ leading to the total amount of $4A_f E_f$ when the four fibres are considered (A_s and E_s are the fibre cross-section and young's modulus, respectively). For convenience, the analysis is carried out relating the total fibre rigidity with the matrix rigidity by assuming $4A_f E_f = \alpha A_m E_m$. A rather fine 2D solid boundary mesh with 60 linear elements, also shown in Figure 5, was adopted to assure obtaining accurate numerical values. Four discretizations, with 25, 50, 100 and 200 elements per fibre, were used to approximate displacements and interface forces. Finer discretizations are required to capture precisely the interface forces near the fibre end where singularity is expected. The example was also analysed by using only boundary elements, treating the fibres as very thin sub-region as proposed by Leite et al.,

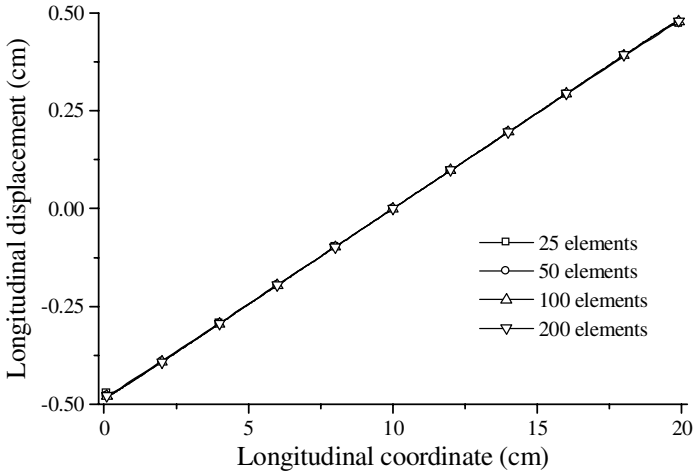

Figure 6 : Longitudinal displacements along a central fibre.

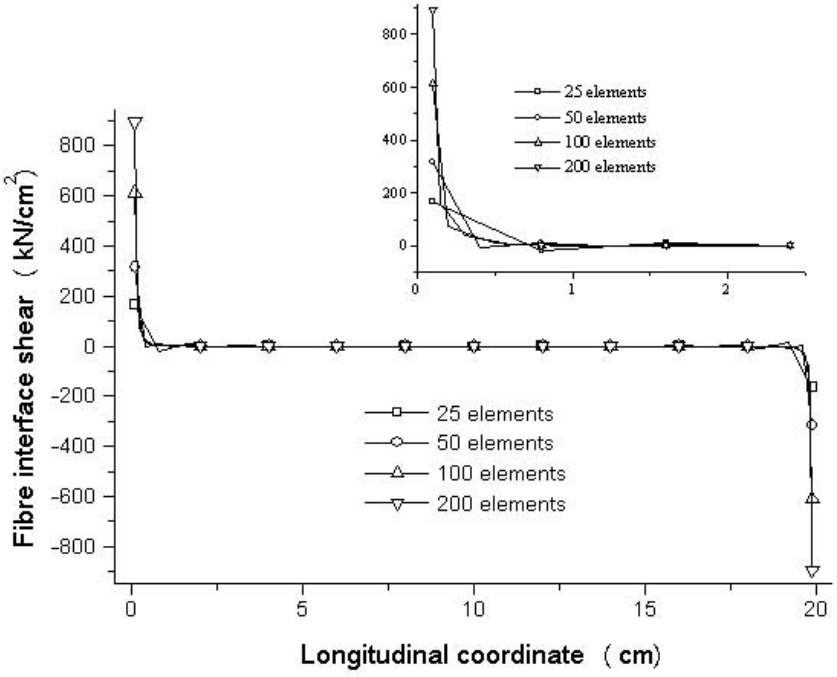

Figure 7 : Fibre-matrix interface shear force distribution.

2003. For this BEM analysis both side of each fibre must be discretized as well as the very small ends.

Figure 6 shows the displacements computed along the beam axis. These results have been obtained by making the parameter $\alpha = 1$, i.e., the matrix and the fibre rigidities are the same. As one can see, accurate results are obtained even for course meshes. For this example, the results obtained by using the standard BEM/FEM and BEM/BEM combinations are also accurate. The interface shear force distributions computed by adopting several fibre discretizations are depicted in Figure 7. A rather fine mesh was needed to represent the unbounded value near the fibre end (fibre end detail in Figure 7). Although unbounded values are expected at the fibre ends and very high values on its vicinity, the force distribution computed for all experimented discretizations are smooth and exhibit the same behaviour. It is important to point out that interface forces exhibiting oscillations may be obtained with the standard BEM/FEM approach, even when reasonable fine meshes were used. The oscillations will disappear only for very fine meshes.

We have also run this problem for several fibre densities to verify the capability of the formulation to deal with highly reinforced domains. We have used four reinforcement densities α =0.5, 1.0, 2.0 and 4.0. Figures 8 and 9 show the influence of the reinforcement densities on the computed results given in terms of longitudinal displacements and shear force along the fibre-matrix interface.

The second example analysed here was carried out to check the capability of the formulation to model the bonding shear stress distribution along the steel bar-matrix interface during a classical pulling test. In Figure 10, a steel bar is partially embedded into a 2D block; a small part of the steel bar is not immersed to allow applying the pulling forces. The geometric data chosen to perform this analysis is also given in Figure 10. Displacements are prescribed equal to zero along the left vertical side of the two-dimensional domain, whereas at the opposite side the load is applied by prescribing the displacement u_f at the steel bar extremity; the 2D domain right end is free to move. The concentrated force P, the prescribed displacement u_f conjugate, acts to pull the steel bar out of the domain.

The elastic properties assumed for this analysis are: block Young's modulus, E_m=30,000.00Mpa, Poisson's ratio ν=0.0, steel bar rigidity, $E_f A_f = 21,000.00$ kN. The debonding model parameters chosen to run this example are: $\alpha = 0.8$, $s_1 = 0.06\,cm$, $s_2 = 0.065\,cm$, $s_3 = 0.1\,cm$, $f_{\max} = 10.95\,MPa$ and $f_f = 1.65$MPa. A boundary mesh with 60 linear elements is adopted to approximate the matrix domain boundary, while 160 uniform finite elements were adopted to model the single steel bar. Finer meshes have been tested to confirm that the discretization adopted was enough fine to give accurate results.

Figure 11 shows the obtained force-displacement $(P\,X\,u_f)$ curve. As expected, one has a non-linear response due to the sliding effect. Initially, the curve is almost linear. Then, the bonding strength diminishes and the steel bar slides.

Figure 12 shows five different diagrams with the debonding forces acting along the steel bar, each one for a particular value of the prescribed displacement u_f. As expected, for low values of u_f, the forces are larger in the vicinity of the steel bar end. As u_f increases, one can observe that the horizontal path of the debonding model was clearly represented. Prescribing a large displacement, as $u_f = 0.15\,cm$, the interface shear forces reach the limit $f_f = 1.65\,MPa$ along the whole steel bar interface. Figures 13 and 14 show the matrix displacement u and the slip s along the steel bar interface, respectively, for different values of the prescribed displacement u_f. As shown in Figure 13, the matrix displacements increase along the whole steel bar when u_f increases. For $u_f = 0.15\,cm$, the matrix displacements decrease as a result of the debonding model softening. On the other hand, the slip values given in Figure 14 always increase when u_f increases, as expected.

Conclusions

In this work an improved BEM/FEM coupling is presented to deal with reinforced 2D elastic domains considering the possibility of sliding along the matrix-fibre interface. The combination of the two methods is made by writing redundant algebraic equations. The necessary number of algebraic relations is then obtained by using the least square method. A non-linear criterion has been introduced to allow sliding between the reinforcement and the matrix material. For this case the consistent tangent operator has been derived. For the solution of the non-linear system an implicit scheme was adopted. The accuracy and reliability of the developed formulation to deal with reinforced domains have been demonstrated by solving two rather complex examples.

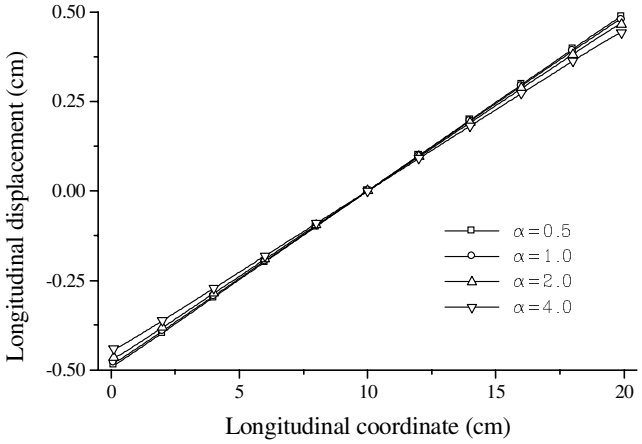

Figure 8 : Longitudinal displacements along a central fibre for several reinforcement densities.

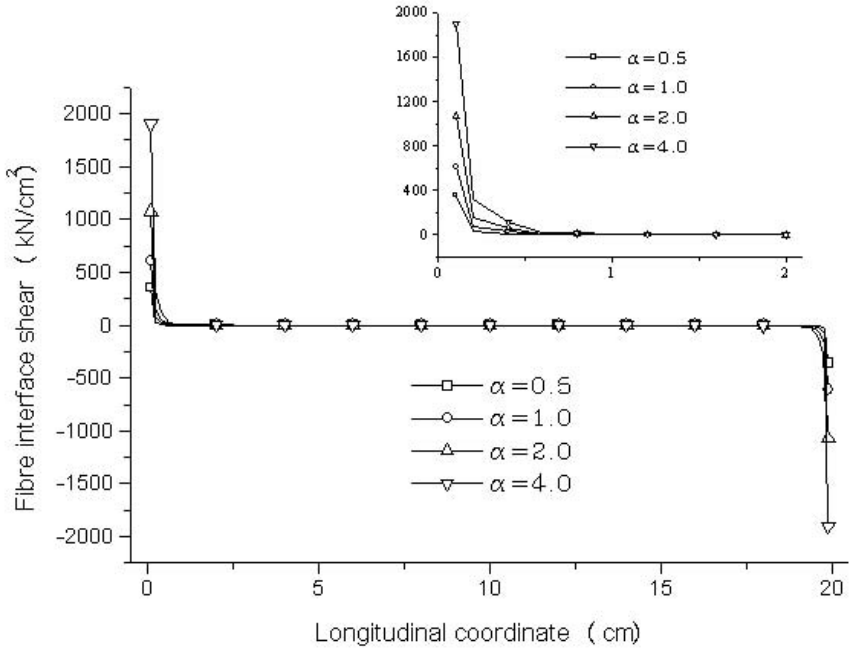

Figure 9 : Fibre-matrix interface shear force distribution for several reinforcement densities.

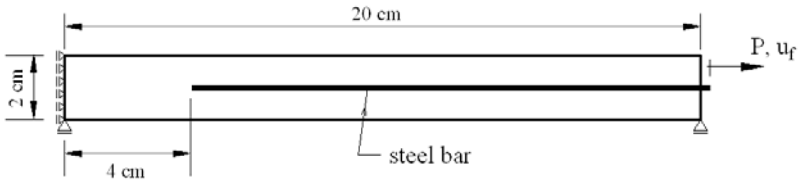

Figure 10 : Reinforced 2D domain.

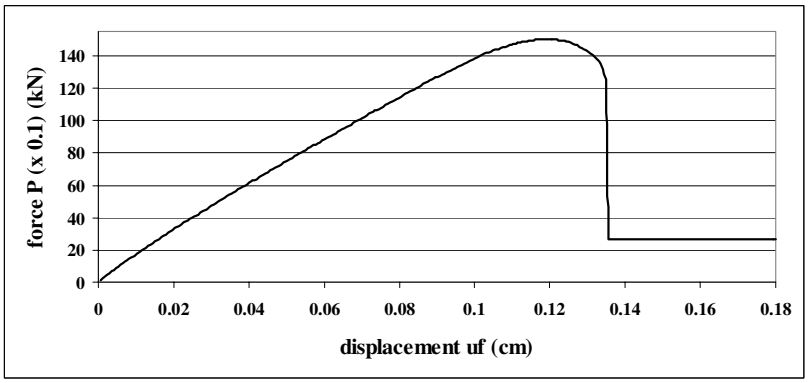

Figure 11 : Force-displacement curve.

Acknowledgement: The author wishes to thank FAPESP (São Paulo State Foundation for Scientific Research).

References

Atluri, S.N.; Han Z.D.; Shen, S. (2003): Meshless Local Petrov-Galerkin (MLPG) approaches for solving the weakly-singular Traction & displacement boundary integral equations, *CMES: Computer Modeling in Engineering & Sciences*, vol. 4, no. 5, pp. 507-518.

Bonnet, M.; Maier, G.; Polizzotto, C. (1998): Symetric Galerkin boundary element method, *Appl. Mech. Rev*., vol. 51, pp. 669-704.

Brebbia, C.A.; Dominguez, J. (1992): *Boundary elements: an introductory course*, Comp. Mech. Publ., Southampton.

Coda, H.B.; Venturini, W.S. (1995): Three-dimensional transient BEM analysis, *Computer & Structures*, Vol. 56, no. 5, pp. 751-768.

Coda, H.B.; Venturini, W.S. (1999): On the coupling of 3D BEM and FEM frame model applied to elasto-dynamic analysis, *International Journal of Solids and Structures,* vol. 36, no. 31-32, pp. 4789-4804.

Coda, H.B.; Venturini, W.S.; Aliabadi, M.H. (1999): A general 3D BEM/FEM coupling applied to elastody-namic continua/frame structures interaction analysis, *International Journal for Numerical Methods in Engineering*, vol. 46, no. 5, pp. 695-712.

Coda, H.B. (2001): Dynamic and static non-linear analysis of reinforced media: a BEM/FEM coupling approach, *Computers & Structures,* vol. 79, pp. 2751-2765.

Comité Euro-International du Béton CEB/FIP Structural Concrete (1999): *Textbook on Behaviour, Design and Performance*, vol. 1.

Cruse, T.A. (1969): Numerical solutions in three-dimensional elastostatics, *International Journal of Solids and Structures,* vol. 5, pp.1259-1274.

Han, Z.D.; Atluri, S.N. (2003) a: On simple formulations of weakly-singular traction & displacements BIE, and their solutions through Petrov-Galerkin Approaches, *CMES: Computer Modeling in Engineering & Sciences*, vol. 4, no. 1, pp. 5-20.

Han, Z.D.; Atluri, S.N. (2003)b: Truly Meshless Local Petrov-Galerkin (MLPG) solutions of traction & displacements BIEs, *CMES: Computer Modeling in Engineering & Sciences*, vol. 4, no. 6, pp. 665-678.

Leite, L.G.S.; Coda, H.B.; Venturini, W.S. (2003): Two-dimensional solids reinforced by thin bars using the boundary element method, *Engineering Analysis with Boundary Elements*, vol. 27, no. 3, pp.193-201.

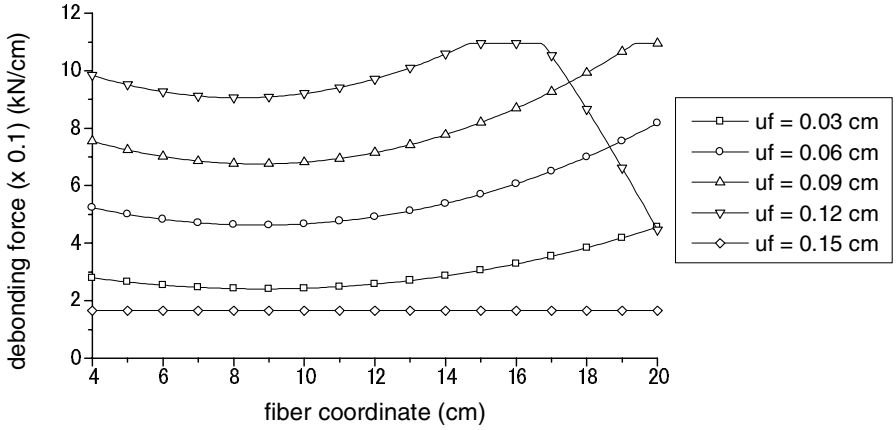

Figure 12 : Debonding forces along the steel bar for different values of u_f.

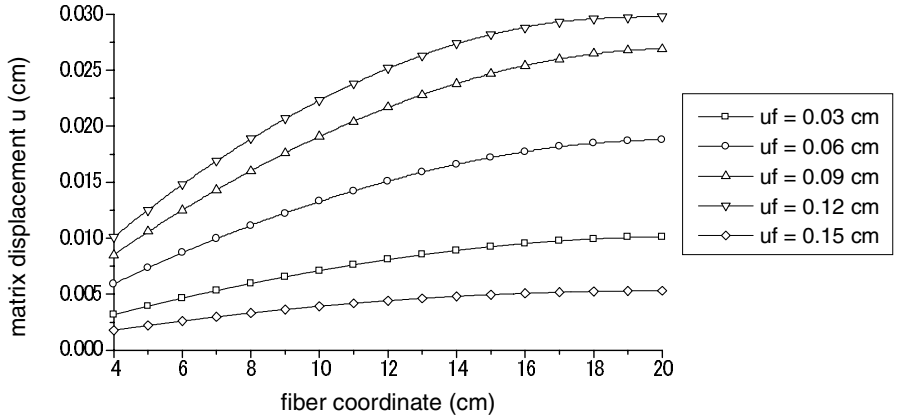

Figure 13 : Matrix displacement *u* along the steel bar for different values of u_f.

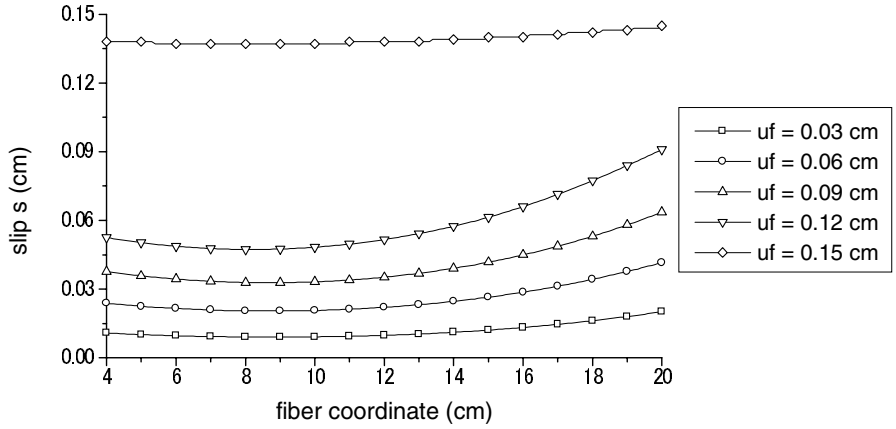

Figure 14 : Slip *s* along the steel bar for different values of u_f.

Okada, H.; Rajiyah, H.; Atluri, S.N. (1989)a: A novel displacement gradient boundary element method for elastic stress analysis with high accuracy, *Journal of Applied Mechanics,* April 1989, pp. 1-9.

Okada, H.; Rajiyah, H.; Atluri, S.N. (1989)b: Non-hyper-singular integral representations for velocity (displacements) gradients in elastic plastic solids (small or finite deformation), *Computational Mechanics*, vol. 4, pp.165-175.

Osias, J.R.; Wilson, R.B.; Seitelman, L.A. (1977): Combined boundary integral equation finite element analysis of solids, In: 1^{st} *Symposium on innovative Numerical analysis in applied engineering science*, Versailles, Cetin.

Shaw, R.P.; Falby,W. (1977): A combined finite element-boundary integral equation method, In: 1^{st} *Symposium on innovative Numerical analysis in applied engineering science*, Versailles, Cetin.

Rizzo, P.J. (1967): An integral equation approach to boundary value problems of classical elastostatics, *Quart. Appl. Math.,* vol. 25, pp. 83-95.

Vallabhan, C.V.G.; Sivakumar, J. (1986): Coupling of BEM and FEM for 3D problems in geotechnical engineering. In: 2^{nd} *Boundary Element Technology Conference*, MIT, Massachusetts, USA, *Proceedings*, 675-686.

Venturini, W.S. (1992): Alternative formulations of the boundary element method for potential and elastic zoned problems, *Engineering Analysis with Boundary Elements*, vol. 9, no. 3, pp. 203-207.

Zienkiewicz, O.C., Kelly, D.W. & Bettess, P. (1997) The coupling of the finite element method and boundary solution problems. *International Journal for Numerical Methods in Engineering*, 11: 355-375.